

Shining Light at Working Interfaces and Chiral Nanoparticles

Thomas Bürgi*

Abstract: In this article we present an overview of our recent research in the fields of *in situ* spectroscopy, nanomaterials and chirality. Our research focuses around the spectroscopic investigation of chemical reactions taking place at solid–liquid interfaces. This research goes hand in hand with the development of experimental techniques that enable us to study interface phenomena *in situ*. Using such techniques we try to shed light on photocatalytic reactions like the decomposition of organic pollutants in water or the reduction of carbon dioxide. We are moreover interested in chiral surfaces and their ability to discriminate between enantiomers. Again this relies on special techniques that highlight the enantiodiscriminating surface–adsorbate interactions. We furthermore seek to transfer chirality from adsorbates to metal nanoparticles. The latter are probed by chiroptical techniques, particularly also vibrational circular dichroism (VCD). Finally, we aim at preparing metamaterials with tailored optical properties by organizing plasmonic particles in two and three dimensions.

Keywords: Attenuated total reflection · Chiral surfaces · Nanoparticles · Photocatalysis · Spectroscopy



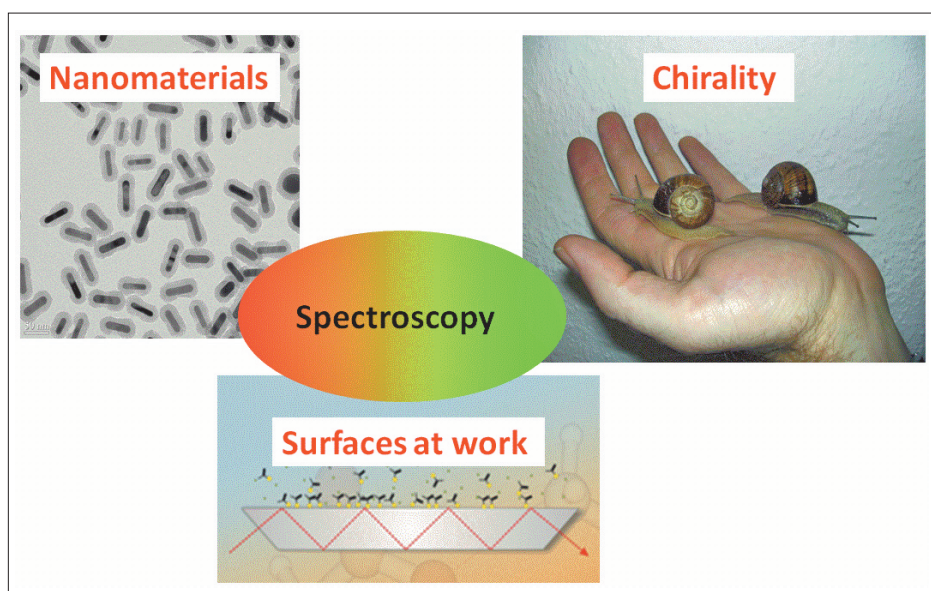
Thomas Bürgi studied chemistry in Bern (Switzerland) and received his diploma in 1991 and his PhD in 1995 on laser spectroscopy (with Prof. S. Leutwyler) After

two years of post-doctoral work (with Prof. S. T. Ceyer) on surface chemistry and physics at the Massachusetts Institute of Technology (MIT) in Cambridge, Massachusetts, he took up a position as an Oberassistent at ETH Zürich, working on the design and characterization of catalytic interfaces and materials. Thomas Bürgi completed his Habilitation in 2002. In 2003 Thomas Bürgi moved to the University of Neuchâtel as a Förderungsprofessor of the Swiss National Science Foundation. His group focused on the preparation of (chiral) nanomaterials and their application in optics, catalysis and as nanofluids. In addition methods to study surface reactions *in situ* were further developed. In 2008 Thomas Bürgi accepted a position as professor of Physical Chemistry at the University of Heidelberg and since 2010 he is professor of Physical Chemistry at the University of Geneva.

Introduction

The research of our group focuses around chemical reactions taking place at solid–liquid interfaces, which goes hand in hand with the development of experimental techniques that enable the study of interface phenomena *in situ*. In particular we are interested in studying interface phenomena relevant for sustainable technologies like photocatalysis, light harvesting and solar energy conversion. In addition, we are interested in the preparation of nanomaterials with tailored (chir)optical properties, their in-depth characterization, their organization in two- and three dimensions and their use for catalytic applications and as metamaterials.

Fig. 1 summarizes our research with the three keywords: Surfaces, chirality and nanomaterials. For all the three research fields spectroscopy plays a key role for us. At first glance the three areas have nothing to do with each other, but this is not true as becomes evident after a second thought. For example, the preparation of nanomaterials and a lot of their properties strongly depend on surface chemistry and physics. On a macroscopic level gravity is the most important force acting on an object. For a nanoscale object surface forces are largely dominating over gravitational forces. This has to do with the fact that the surface to volume ratio increases when the size of an object decreases. For a 2 nm metal particle, for example, 40% of the atoms are located at the surface.



*Correspondence: Prof. Dr. T. Bürgi
Département de Chimie Physique
Université de Genève
Quai Ernest-Ansermet 30
CH-1211 Genève 4
Tel.: +41 22 379 65 52
Fax: +41 22 379 61 03
E-mail: thomas.buergi@unige.ch

Fig. 1. Summary of current research interests.

What has chirality to do with surfaces or nanomaterials? Chiral surfaces are already used for example in enantioseparation or catalysis. For example the use of chiral modified metal catalysts is one strategy for the synthesis of optically pure compounds.^[1]

An interesting scientific question, which impacts on future chiral technology, is how chirality can be transferred from an adsorbate to metal surfaces or nanoparticles. Despite the fact that metals have highly symmetric bulk structure there is evidence that their surface becomes chiral under the influence of an adsorbate. For example, Raval and coworkers have shown that the adsorption of tartaric acid on Ni(100) leads to the distortion of the Ni surface atoms involved in the adsorbate complex resulting in a local chiral arrangement.^[2] Therefore the chiral molecule imparts a 'chiral footprint' onto the metal surface. Similarly, the surface region of gold nanoparticles or clusters can become chiral under the influence of adsorbed thiols, even if the later is not chiral.^[3] The better understanding of such effects will help the development of new chiral materials.

This article gives an overview of our recent and current research. It is tried to convey the principle idea of the respective projects and provide, where appropriate, possible future perspectives.

Spectroscopy of Solid–Liquid Interfaces

The study of chemical processes at interfaces largely relies on suitable techniques that can provide molecular level information of the interface. In order to study chemical reactions at interfaces such information should be gained *in situ* that is, while the process or chemical reaction of interest is taking place. This is an important point because it has been shown in numerous cases that the properties of an interface are not the same before, during and after a certain process (chemical reaction). This insight has led in the past two decades to the development of new techniques capable of studying interfaces at work.^[4]

Our contribution to this field is the further development and application of infrared vibrational spectroscopic methods to study solid–liquid interfaces *in situ*. A vibrational spectrum contains rich information on the adsorbate layer. For example, molecules can be identified or at least functional groups can be recognized. Adsorbates can be quantified, *i.e.* their surface concentration can be determined under certain conditions.^[5] Furthermore, by using polarized light the (average) orientation of adsorbates on flat surfaces can be obtained. The rich information that can

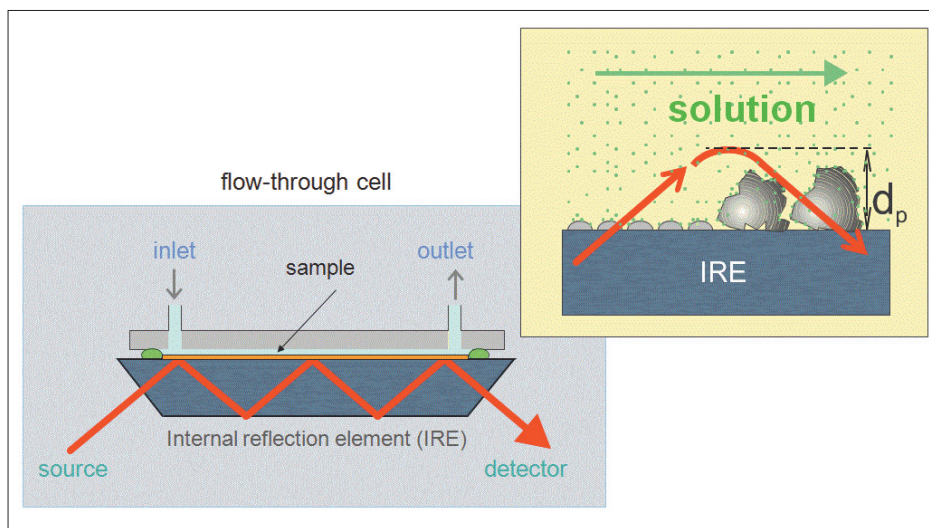


Fig. 2. Principle of attenuated total reflection (ATR) spectroscopy. The evanescent field formed at the interface between internal reflection element and adjacent medium is used for spectroscopy.

be obtained and the fact that infrared (IR) spectroscopy is comparably cheap make the technique attractive for surface and interface studies.

Solid–liquid interfaces are experimentally demanding because one has to discriminate between adsorbates and the liquid phase. Some of the IR geometries and techniques that are used for studying solid–gas interfaces are hardly practical in the presence of a liquid because the IR light absorption of the liquid phase is too strong. One way out of this is to use internal reflection spectroscopy or attenuated total reflection (ATR) IR spectroscopy^[6] (Fig. 2). ATR-IR is based on the total internal reflection of a light beam at an interface formed between two media. The resulting field at the interface is used for spectroscopy. The evanescent nature of this field allows one to probe the layer close to the interface formed between the internal reflection element and the sample. Therefore, the field probes only a small part of the bulk fluid phase, such that molecules at the interface can be studied even in the presence of strongly absorbing solvents such as water. This makes the technique particularly interesting for applications in biology, where water is *the* solvent. The electric field amplitude of the evanescent field falls off exponentially with distance z from the surface as

$$E = E_0 e^{-z/d_p} \quad (1)$$

Here E_0 is the electric field amplitude at the interface, which depends on the angle of incidence, the refractive indices of sample (n_2) and reflection element (n_1) and the polarization of the field. The depth of penetration d_p , defined as the distance

required for the electric field amplitude to decrease to e^{-1} of its value at the surface is given by

$$d_p = \frac{\lambda_1}{2\pi\sqrt{(\sin^2\theta - n_{21}^2)}} \quad (2)$$

where $\lambda_1 = \lambda n_1^{-1}$ is the wavelength in the denser medium and $n_{21} = n_2 n_1^{-1}$ is the ratio of the refractive indices of the rarer and denser medium. For a Ge internal reflection element (IRE, $n_1 = 4$) in contact with water ($n_2 = 1.33$) at an angle of incidence of $\theta = 45^\circ$, the effective thickness at 1640 cm^{-1} is $0.44 \text{ }\mu\text{m}$ for parallel polarized light (polarized in the plane of incidence of the light) and $0.22 \text{ }\mu\text{m}$ for perpendicular polarized light. For a ZnSe IRE the corresponding values are 1.12 and $0.56 \text{ }\mu\text{m}$.

The fact that IR spectroscopy is not selective in combination with the often observed complexity of 'real' interfaces was realized as a significant challenge. Working interfaces are often characterized by several coexisting adsorbates, which results in crowded spectra and overlapping bands. In such situations conventional infrared spectroscopy reaches its limits and it can therefore be crucial to combine it with additional methods or data analysis tools. A method that we have applied successfully is modulation excitation spectroscopy (MES) in combination with phase-sensitive detection^[7] in order to study various heterogeneous catalytic systems,^[8] structural changes within self-assembled monolayer (SAMs)^[9] and enantiodiscrimination at chiral surfaces.^[10]

The principle of modulation excitation spectroscopy is shown in Fig. 3. The sample is stimulated periodically by an external parameter at the stimulation frequency ω (the stimulation is represented as a green

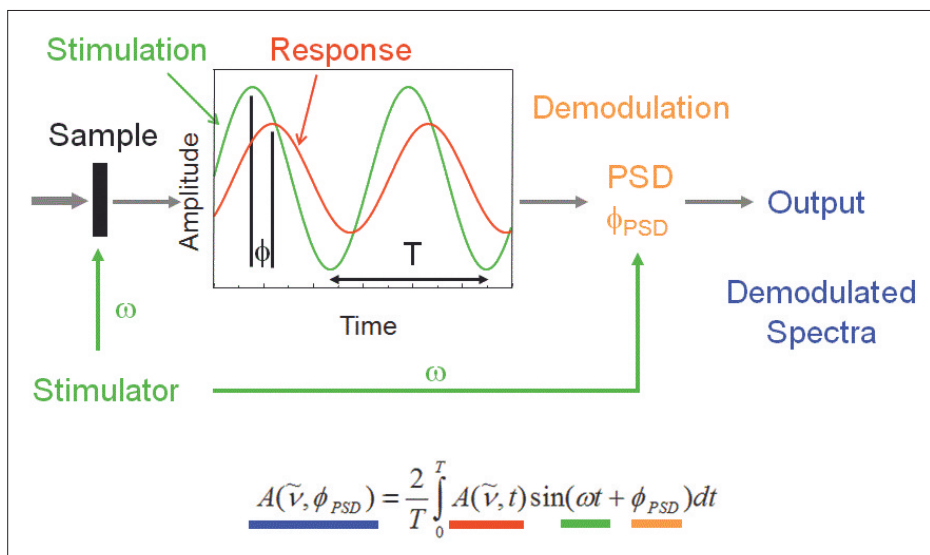


Fig. 3. Principle of modulation excitation spectroscopy.

sinusoidal line). The periodic system response (reversibility provided) due to the stimulation is shown as a red line in Fig. 3. The response can be delayed with respect to the stimulation (phase lag) but, importantly, the frequency of the response will be identical to the stimulation frequency (or harmonics thereof). The resulting absorbance variations $A(\tilde{\nu}, t)$ are followed by measuring spectra at different times during the modulation period T . The signal can be averaged over many periods. The set of time-resolved spectra $A(\tilde{\nu}, t)$ is then transformed by means of a digital phase-sensitive detection (PSD), according to Eqn. (3), to a set of phase-resolved spectra

$$A_k^{\phi_{PSD}}(\tilde{\nu}) = \frac{2}{T} \int_0^T A(\tilde{\nu}, t) \sin(k\omega t + \phi_k^{PSD}) dt \quad (3)$$

where $k = 1, 2, 3, \dots$ determines the demodulation frequency, *i.e.* fundamental, first harmonic, and so on, T is the modulation period, $\tilde{\nu}$ denotes the wavenumber, ω the stimulation frequency and ϕ_k^{PSD} the demodulation phase angle. With a set of time-resolved spectra $A(\tilde{\nu}, t)$, Eqn. (3) can be evaluated for different phase angles ϕ_k^{PSD} resulting in a series of phase-resolved spectra $A_k^{\phi_{PSD}}$.

A prerequisite for the application of MES is the reversibility of the system under investigation. On the other hand the advantages of MES over conventional spectroscopy are manifold. The signals in the demodulated spectra are exclusively related to the stimulation of the external parameter, *i.e.* MES selectively highlights the species that are affected by the external parameter and suppresses static signals from species that do not respond to the stimulation. Furthermore, demodulated

spectra are of much higher quality with a better signal-to-noise ratio. The kinetic information of the investigated system is contained in the frequency-dependent amplitude of the response and the phase lag between stimulation and response (see Fig. 3). Consequently, species with different kinetics can be separated by setting the demodulation phase angle ϕ_k^{PSD} accordingly, which also allows the detection of minor species.

We have applied the combination of ATR-IR and modulation excitation spectroscopy to the investigation of photocatalytic reactions triggered by the illumination of TiO_2 . With sufficiently large photon energy electrons can be excited across the band gap of the semiconductor creating electron-hole pairs. The electrons and holes can then migrate the surface of the TiO_2 particles and induce chemical reactions in the adsorbed molecules. The holes can directly oxidize adsorbed organic molecules. The electrons can be accepted by atmospheric oxygen molecules to form reactive oxygen species such as superoxide anions or hydroperoxo radicals. The latter can then also attack organic molecules.

ATR-IR in combination with modulation excitation spectroscopy allows one to follow the changes occurring on the TiO_2 surface induced by illuminating the semiconductor, for example during the decomposition of organic molecules. In order to apply ATR-IR the TiO_2 has to be brought in contact with the internal reflection element (IRE), which can be achieved by preparing a film of the TiO_2 nanopowder on the IRE for example by spin coating. The thickness of the film should ideally be on the order of the penetration depth of the light. Much thicker films can lead to significant diffusion times. In a typical experiment the film is then exposed to a flowing solution

of the molecule that is to be studied. After adsorption of the molecule on the TiO_2 surface light modulation experiments can be performed by turning on and off the UV light used to excite the TiO_2 semiconductor, for example by using a shutter.

Using this experimental strategy we investigated the decomposition of malonic acid over TiO_2 .^[11] The spectra obtained after adsorption of the molecule in the dark lead us to conclude that the molecule is adsorbed as malonate with its two carboxylate groups interacting differently with the surface *i.e.* one as a bidentate and the other one in a monodentate binding mode. This leads to two bands for the symmetric and two bands for the anti-symmetric carboxylate stretching mode. Interestingly, for succinic acid (two methylene groups between the acid groups instead of one as in malonic acid) only one band was observed for the carboxylate vibrations, indicative of similar interaction modes of the two carboxylate groups with the TiO_2 surface (bidentate). Illuminating the adsorbed malonate at full coverage (in a continuous flow of malonic acid solution, 1.5×10^{-4} mol/l), its signals became weaker and bands associated with oxalate grew in, as can be seen from Fig. 4, where the signals of malonate and oxalate are shown as a function of time for different conditions (light on/off, concentration of malonic acid in solution). When shutting off the light additional malonate adsorbed, whereas the adsorbed oxalate remained on the surface. This observation has led us to the conclusion that during the photocatalytic process a large fraction of the TiO_2 surface is not covered by the acids (under the applied conditions). The transformation of malonate to oxalate as observed by conventional ATR-IR experiments is the result of a decarboxylation (photo-Kolbe reaction) leading to a first CO_2 molecule, and a subsequent conversion of the carbon-centered radical to a carboxylic group (see Fig. 5). The whole process is initiated by the injection of a photogenerated hole into the adsorbed malonate. When adsorbed oxalate is further illuminated it is reacting with two holes to yield two further CO_2 molecules. The concomitant removal of oxalate from the TiO_2 surface can easily be observed by ATR-IR (see Fig. 4).

To get even more information we have performed light modulation experiments. The higher sensitivity allowed us to observe the dissolved CO_2 that is formed in the photocatalytic experiments, as can be seen in Fig. 5 (right), although the experiments were conducted under flow-through conditions. By using selectively ^{13}C labeled malonic acid, with the label in the middle position, and by measuring the relative abundance of CO_2 and $^{13}\text{CO}_2$ we determined that about 50% of the photo-

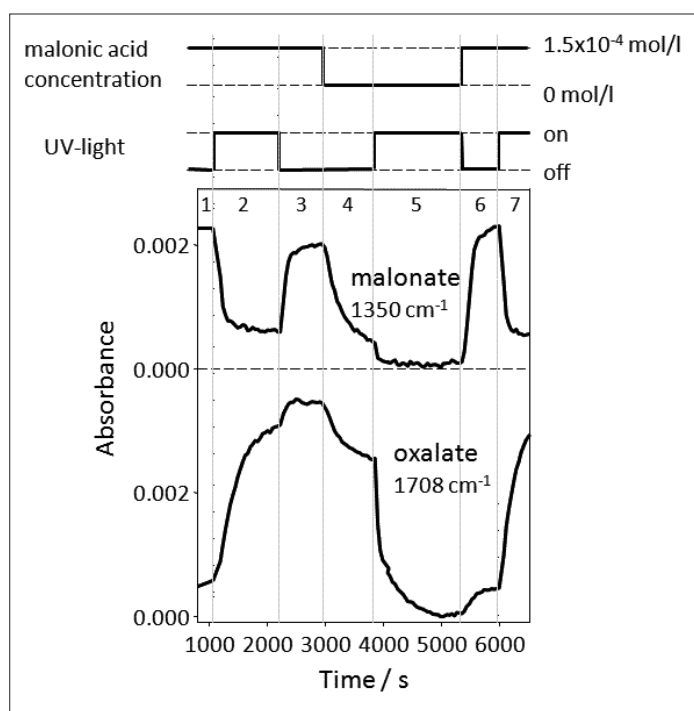


Fig. 4. Absorbance at 1350 (malonate) and 1708 cm^{-1} (oxalate) as a function of time as followed by ATR-IR spectroscopy during different treatments of a TiO_2 film with UV light and malonic acid solution. Reprinted with permission from ref. [11]. Copyright 2006 American Chemical Society.

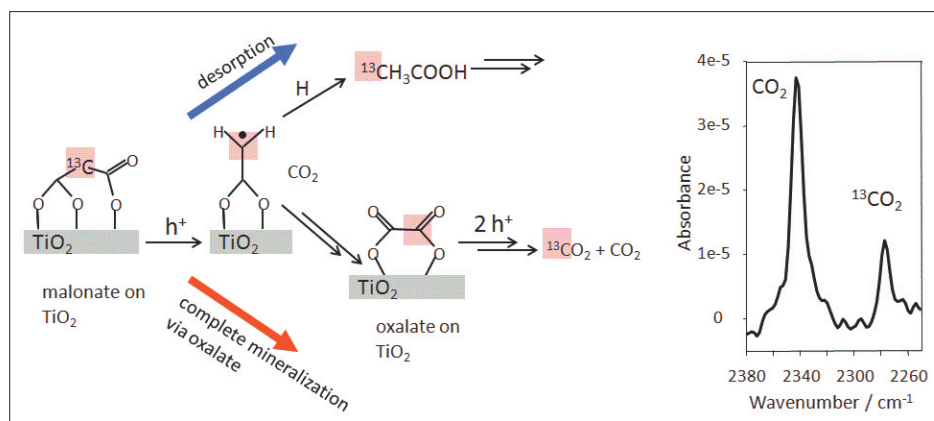


Fig. 5. Left: Mechanism of photocatalytic decomposition of malonic acid over TiO_2 . Right: Demodulated ATR-IR spectra showing dissolved CO_2 (labeled and unlabeled). Reprinted with permission from ref. [12]. Copyright 2007 Elsevier Science.

catalytic decomposition of malonic acid runs through an oxalate intermediate. The other 50% proceeds *via* a C_2 species that is desorbing into solution after the initial decarboxylation step, as schematically depicted in Fig. 5.^[12]

With the help of the modulation technique it was also possible to observe minor species on the TiO_2 surface that could not be observed by conventional ATR-IR spectroscopy. In order to do so one has to choose the appropriate demodulation phase angle ϕ_k^{PSD} (Eqn. (3)). The amplitude of the spectral signals of a species vary with the demodulation phase angle. For a certain demodulation phase angle the signals are maximal ('in phase'). This phase angle might be different for different species, depending on their kinetics. The addition of 180° to this demodulation phase angle leads to minimal (negative) signals. By choosing the demodulation phase angle

90° larger or smaller leads to zero amplitude signals, *i.e.* they vanish. Therefore, by choosing the demodulation phase angle appropriately leads to the complete cancellation of the most dominant signals in the spectrum, in our case the signals of the adsorbed malonate. Signals from minor species then remain, which are otherwise not observed. In the case of malonic acid decomposition it became evident that carbonates are adsorbed on TiO_2 during photocatalysis. These carbonates are very stable on the surface in the dark but diminish upon illumination. It is likely that the carbonates are formed through the re-adsorption of the reaction product CO_2 . The carbonates influence the overall reaction by blocking adsorption sites and by competing with the reactant for reactive species.

Using the same experimental strategy we also investigated the photocatalytic decomposition of some amino acids.^[13] This

is important since photocatalysis by TiO_2 is considered as a method for treatment of water polluted by biological waste. Of special interest was the question concerning the fate of the nitrogen atom of the amino acids. In former studies ammonia and also nitrates were evidenced in the liquid phase.^[14] Horvath and co-workers studied the photodegradation of aspartic acid over bare and silver loaded TiO_2 and found that the nitrogen contained in the amino acid is predominantly converted into NH_3 and after prolonged irradiation into NO_3^- .^[14] Our own ATR-IR experiments evidenced the formation of cyanide (CN^-)! The observation of cyanide is certainly an important finding in view of the application of photocatalysis for water cleaning.^[13]

Metal nanoparticles on the TiO_2 act as sink for the photogenerated electrons thus increasing the lifetime of the hole and the photocatalytic activity. We therefore studied the photocatalytic decomposition of amino acids on TiO_2 decorated with gold nanoparticles, TiO_2/Au .^[13] The cyanide formed during illumination strongly adsorbed on the gold and led to its leaching into the solution, as evidenced by mass spectrometry. ATR-IR light modulation excitation spectroscopy furthermore revealed that the electrochemical potential of the gold particles changed when turning on/off the light. This was possible due to the fact that the C–N stretching frequency of cyanide adsorbed on gold depends on the state of the gold particles, *i.e.* whether they are electron-rich or not. Upon illumination the photo-generated electron in the conduction band in the TiO_2 is transferred to the gold nanoparticles. The latter get electron-rich, which can be sensed by the frequency of the adsorbed cyanide. From the frequency shift the change of the potential of the gold nanoparticles upon illumination could be estimated to be about 0.4 eV.

Photocatalysis can not only be used to decompose organic molecules (*e.g.* pollutants) to CO_2 and water. The reverse reaction is even more attractive. Fossil fuels are a limited resource and their burning influences the global climate. Until regenerative methods like photovoltaic processes can replace fossil fuels alternative technologies that are compatible with existing infrastructure (motors, pipelines) are attractive. The reduction of CO_2 to for example methanol is an appealing way to convert sunlight into fuel. Advantages of such a technology would be the CO_2 neutrality, the ability to store the fuel and use of existing infrastructure. Challenges are the currently low efficiency of the process.

TiO_2 has its band-gap energy in the UV region of the spectrum. In order to use the visible part of the solar spectrum we use dye-sensitized TiO_2 . Analogous to the initial charge separation in a dye-sensitized

solar cell^[15] an (organic) dye, after light absorption, injects an electron into the conduction band of the semi-conductor. This electron is then available for the reduction of CO₂. The dye has to be regenerated through electron transfer from a redox mediator. The ultimate goal is the use of water as the reductant according to:



The redox mediator transfers oxidation equivalents to an oxidation catalyst, which then oxidizes water to oxygen. In the field of water oxidation important progress has been made recently.^[16]

The reduction of carbon dioxide to methanol is a multi-step six-electron reaction. The main challenge is not so much the transfer of the electron from the dye to the semiconductor but the availability of catalytic sites and the transfer of the electron to these sites. TiO₂ alone is not a very efficient catalyst, but the addition of metal nanoparticles, particularly copper, leads to an improvement of the efficiency.

We again used ATR-IR spectroscopy to study these catalytic systems. The method provides important information about the anchoring of the dye to the surface, *i.e.* its adsorption mode, the stability of the dye upon irradiation and the possibility to co-adsorb the reactant (CO₂). When a (dye-sensitized) TiO₂ surface is exposed to CO₂ dissolved in water the surface is covered by carbonates. It seems that dye adsorption does not hinder severely the CO₂ adsorption and CO₂ does not displace the dye from the surface. Under visible light illumination the carbonate signals decrease and signals of reaction intermediates appear in the spectra. Future investigations will focus on the correlation of information obtained from the interface by *in situ* spectroscopy with information from the liquid phase obtained by chromatography.

In photocatalysis much effort is devoted to the development of materials with increased efficiency. For example, by incorporating other elements into TiO₂ additional energy levels within the band gap could be generated or the band gap could be reduced. Unexpected effects might arise from the structuring of the material itself for example in the form of photonic crystals or inverse photonic crystals. These materials are characterized by an energy range where the propagation of light is completely forbidden (photonic band gap). At the high and low energy edges of this photonic band gap, the light exists as standing waves commensurate with the periodicity of the structured material. At these conditions light harvesting can be drastically enhanced and therefore the efficiency of

the photocatalyst increased. In addition to their enhanced light harvesting properties the structuring of the catalyst will be advantageous for mass transport.

Since photons drive the reaction in photocatalysis the intensity of the light acting on the photocatalyst is important. Using plasmonic metallic particles the local electric field can be drastically enhanced. This finds application in the sensitive detection of molecules by surface enhanced Raman scattering (SERS). Whether such enhancement effect might also be used for photocatalysis will be in the focus of future research.

Nanomaterials

Plasmonic particles, a colorful subject at the interface between chemistry and physics, have potential applications in a variety of disciplines such as cancer treatment,^[17] sensing,^[18] imaging,^[19] high density optical storage,^[20] nanofluids,^[21] manipulation of local electric fields or metamaterials.^[22] Perhaps the oldest application of such particles is as pigments. They were used as pigment of ruby-colored stained glass dating back to the 17th century. The red coloration of gold nanoparticles (GNPs) arises from their surface plasmon resonance (SP) due to the coherent oscillation of surface electrons when interacting with incident electromagnetic radiation.

The extinction spectrum of metal nanoparticles depends on several factors, notably their size and shape but also on the optical properties of the surrounding. Also, plasmons of neighboring particles can couple and therefore the appearance of the macroscopic sample depends on the local arrangement of the particles. This is why the self-assembly of nanoparticles into different structures is an important topic.

The first step towards all the fascinating fields mentioned above is the preparation of suitable materials. For most applications the synthesis of monodisperse particles, *i.e.* particles with the same size and shape, is critical. A further challenge is the stability of the material.

Protocols for the preparation of metal nanoparticles of different size and shape were developed recently and their plasmonic resonances studied.^[23] Gold nanorods (GNRs) are attractive particles showing two plasmons, one polarized along the long axis of the rod at longer wavelength and one perpendicular to it at shorter wavelength. The longitudinal plasmon can be tuned over the visible spectral range into the near infrared region of the spectrum by increasing the aspect ratio (length divided by width). The intense plasmon absorption bands of GNRs with peak extinction co-

efficients up to $6.4 \times 10^9 \text{ M}^{-1} \text{ cm}^{-1}$ make GNRs promising candidates for the coloration of bulk materials. In the visible spectral region the coloring strength of GNRs is 4 to 8 times higher than that of commercial organic pigments.^[24]

We have exploited the well known Ag-assisted seed synthesis for the preparation of GNRs.^[25] This method relies on the growth of initially small spherical gold nanocrystals (the seed, about 5 nm in diameter) in the presence of silver ions and an excess of a surfactant (cetyl trimethylammonium bromide, CTAB). Fig. 6 shows a TEM image of the prepared rods, which have an average length and width of 50 nm and 12 nm, respectively and thus an aspect ratio of 4.2. The GNRs were subsequently encapsulated in a mesoporous silica shell of around 15 nm thickness using an optimized Stöber method.^[26] The silica coating makes the GNR@SiO₂ soluble in alcohols, allows engineering their surface properties *via* the versatile silica surface chemistry, improves their thermal stability and may preserve their color after insertion in different media. The silica surface was furthermore modified with octadecylsilane (ODS) in order to disperse the GNRs@SiO₂ in apolar media.^[24]

The encapsulation of GNRs by silica protects the GNRs from aggregation, from thermal coalescence and from thermal rod-to-sphere shape transition. The latter was observed by increasing the temperature of the rods either in an oven or by laser irradiation.

Fig. 6 shows a transmission electron microscope (TEM) image of the GNRs@SiO₂. It can be seen that the initial aspect ratio is preserved during the SiO₂ coating and that the thickness of the latter is *ca.* 15 nm. Fig. 6 also shows the extinction spectra of the CTAB-coated and the silica-coated GNRs. The weak band at 520 nm corresponds to the transverse plasmon, whereas the strong band above 800 nm is linked to the longitudinal plasmon. Using an optimized seed-mediated procedure we obtained high quality GNRs with aspect ratios up to 30 and a longitudinal plasmon band at about 6 μm .^[27]

Compared to the initial GNRs covered by CTAB, the GNRs@SiO₂ showed a shifted longitudinal plasmon resonance (shift from 820 nm to 840 nm) and the absorbance slightly increased due to the rise of the local refractive index around the GNRs (Fig. 6). Upon careful inspection the TEM images indicate a porous SiO₂ layer. This was confirmed by N₂ adsorption-desorption isotherms which revealed a high surface area of 303 m²·g⁻¹ and a bimodal pore size distribution. Analysis using the BJH (Barrett-Joyner-Halenda) method^[28] revealed 3–4 nm pores, corresponding to pores within the SiO₂ layer, besides the

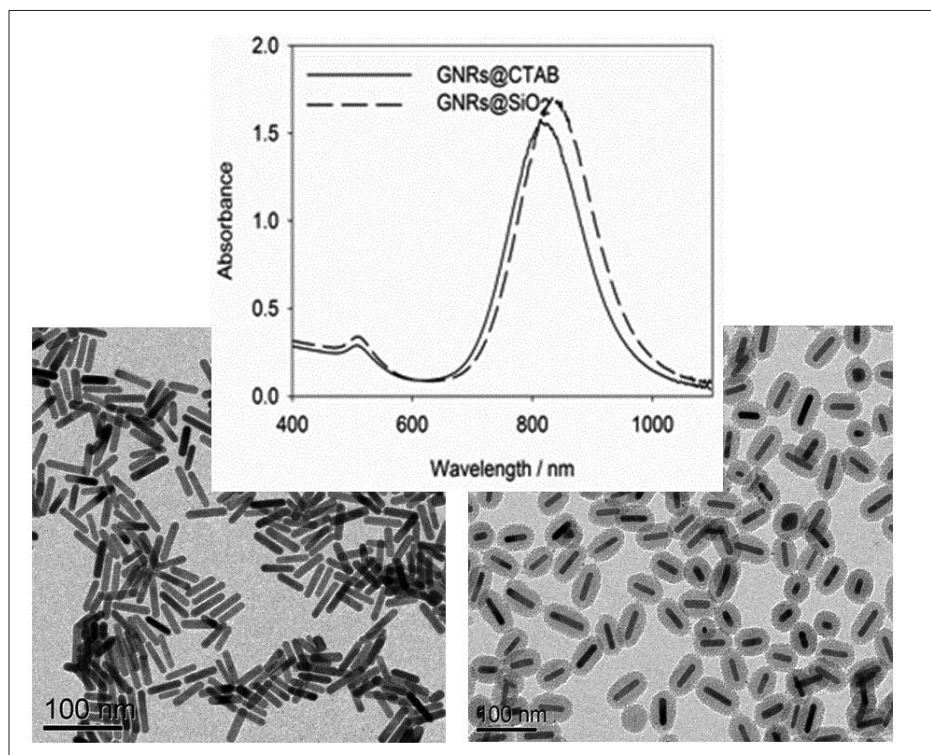


Fig. 6. Transmission electron microscopy (TEM) image and UV-vis spectra of gold nanorods (GNRs) before and after coating with SiO_2 . Reprinted with permission from ref. [24]. Copyright 2010 World Gold Council.

larger pores formed between the individual GNRs@ SiO_2 . The porosity of the SiO_2 shell is likely due to the remaining CTAB during the preparation of the silica shell. CTAB forms micelles in water and is commonly used for the preparation of ordered meso-porous silica.^[29] Interestingly, capillary condensation within the silica shell is sensed by the gold nanorod and leads to a color change of the material, which can therefore ‘sense’ different humidity levels. Using tiny quantities of the GNRs@ SiO_2 described above different plastics were successfully colored using a high volume manufacturing process (extrusion).^[24]

For various applications the thermal stability of GNRs is of importance in order to withstand different processing conditions. Thermodynamically a gold nanorod is not stable. Due to the large energy of cohesion and high surface tension of gold the surface energy becomes an important factor. A metal particle can minimize surface energy by minimizing the surface area and therefore a tendency to form spherical particles is observed. Heating the CTAB-covered GNRs shown in Fig. 6 (left) to 260 °C for 90 minutes led to the complete disappearance of the longitudinal plasmon band and electron microscopy confirmed a transformation from rods to spheres. This shape transformation also allows the selective re-shaping of rods by short laser pulses, by depositing energy into the longitudinal plasmon and therefore heating up the rods. Short pulses are

needed because the local temperature rise in the gold rods is determined by a balance between energy deposited and energy dissipated. Using pulses shorter than the typical time for heat transfer from the rods to the surroundings efficient heating can be achieved. Out of an ensemble of gold nanorods with different aspect ratio (wavelength of the longitudinal plasmon) and different orientation (longitudinal plasmon is polarized along the long axis) one can select the nanorods that undergo melting and rod-to-sphere transformation by choosing the wavelength and polarization of the laser light. Following this strategy multi-dimensional optical recording has been demonstrated.^[30]

The preparation of well-defined nanoparticles has made impressive progress in recent years (and is still continuing to do so). For many applications it is furthermore required to organize the particles for obtaining the desired effect. Plasmonics and metamaterials can be mentioned, where research has focused both on top-down (lithographic) methods as well as bottom-up (self-assembly) approaches. Using the former strategy structures can be made by design, which can however be costly, especially if the structures have to be small. Self-assembly approaches are therefore highly desirable. The preparation of metamaterials is one such research topic where the self-assembly of plasmonic particles could have a large impact.

Metamaterials are a novel kind of artificial matter composed of unit cells which exhibit response characteristics that are not observed in the individual responses of the materials that constitute the metamaterial. If the unit cell is much smaller than the wavelength of light, effective properties like permittivity or permeability can be attributed to the medium which are experienced by the propagating wave field. The most fascinating class of metamaterials is probably those exhibiting simultaneously negative permittivity and permeability, *i.e.* a negative refractive index.^[31] This opens the possibility to develop new functionalities and improvements of electronic and optical devices and components, with performances beyond the physical limit of natural materials. For example, metamaterials exhibiting a negative refractive index can lead to lenses focusing below the diffraction limit or devices that permit objects to be hidden from an external observer (cloaking).^[32]

Metamaterials have been demonstrated for the longer wavelengths of the spectrum by using top-down preparation methods. To move on to the visible spectral range smaller structures are needed, which are hardly accessible or which could not be produced in appreciable quantities at affordable prices by lithography. Our goal is the preparation of metamaterials by self-assembly routes. Such an approach is based on the coupling of plasmons of individual nanoparticles within larger structures. Concepts like the meta-metamaterial^[22] or the core-shell system^[33] have been proposed and it has been demonstrated theoretically that the scattering response of a cluster of metallic nanoparticles sustains a strong magnetic dipole moment. One could understand these materials as media which show strong dispersion in the permittivity in close vicinity to the plasmon resonance of the nanoparticles. Forming a sphere out of such a material allows observation of a strong Mie resonance at slightly larger wavelengths. The lowest order Mie resonance is associated with a magnetic dipole.^[34] The amorphous arrangement of such spherical clusters in space would induce dispersion in an isotropic effective permeability. This property is usually at the focus of interest since it cannot be observed in natural occurring media at optical frequencies.

The concept of meta-metamaterials can be described as follows:^[22] Starting with a small metallic nanosphere it is possible to excite a localized plasmon at appropriate wavelength. The latter depends primarily on the material’s intrinsic dispersion. The dense packing of such spheres allows one to obtain a metamaterial with strong dispersion in the effective permittivity. By forming again spheres out

of such matter, permits for the excitation of Mie resonances in the magnetic mode in the spectral domain where the permittivity of the metamaterial is strongly positive. Arranging these spheres in a densely packed array allows ultimately a medium to be obtained where the effective permeability is strongly negative, reaching values as low as -1 .

Working towards the experimental realization of such materials we organized gold nanoparticles in surfactant matrices. We observed structures analogous to the ones proposed for meta-metamaterials in a mixture of gold nanoparticles with triethyleneglycolmono-11-mercaptoundecylether (EGMUDE) in water.^[35] EGMUDE consists of a thiol, used to anchor to the gold nanoparticle surface, a hydrophobic alkyl chain and a hydrophilic ethyleneglycol part.

The gold nanoparticles were first prepared using the Turkevich-Frens method,^[36] leading to stable diluted gold nanoparticles. In this study we considered 17 nm and 40 nm particles. In a second step EGMUDE was added. Upon addition a fast color change from purple to dark blue and sedimentation was observed, which is usually indicative of nanoparticle agglomeration. However, after some time (several hours without shaking) the sample changed color again. UV-visible spectra showed a strongly red-shifted plasmon resonance (Fig. 7) and dynamic light scattering revealed the formation of larger assemblies of gold nanoparticles, which was then also confirmed by transmission electron microscopy (TEM, see Fig. 7). These entities represent hierarchical structures composed of gold nanoparticles clustered together into larger aggregates of about one μm . Several of these entities again cluster together to an even larger units. Thus these structures strongly resemble the proposed meta-metamaterials. The assembly of the nanoparticles is guided by the EGMUDE, which also stabilizes the particles.

The formation of these clusters of particles is the most obvious reason for the strongly red-shifted plasmon resonance (Fig. 7). In order to better understand the optical response calculations were performed on analogous structures by applying analytical solutions of Maxwell's equations for particles with a spherical symmetry, well-known as Mie-theory, which was extended to handle aggregates of spheres.^[37] With this method one can calculate all quantities of interest for clusters consisting of arbitrarily arranged nanoparticles with a spherical shape. Such calculations very well reproduced the shifted plasmon resonance and furthermore indicated that the dominating contribution to this spectral feature arises from a magnetic dipole oscillation that is induced due to the spheri-

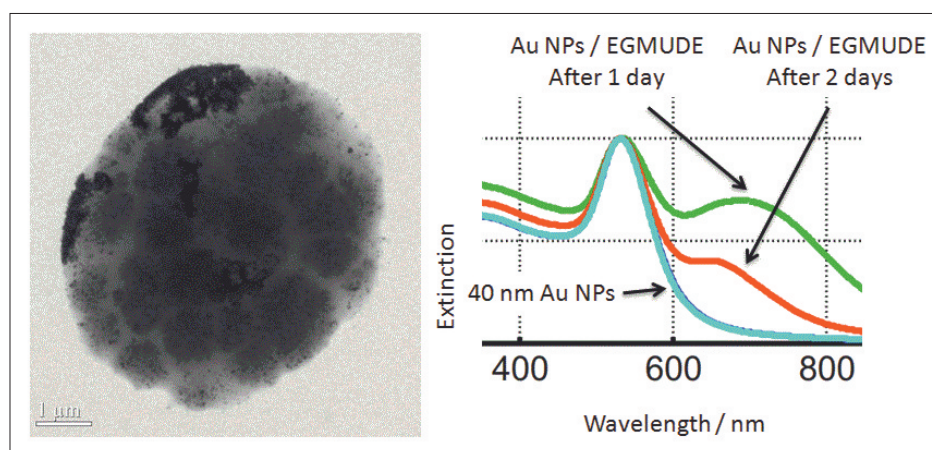


Fig. 7. Transmission electron microscopy (TEM) image and UV-vis spectra of gold nanoparticle (40 nm) EGMUDE assemblies. Reprinted with permission from ref. [35]. Copyright 2009 Royal Chemical Society.

cal shape of the fabricated supramolecular clusters. A dispersive behavior in the effective permeability was furthermore revealed.^[38] Calculations will in the future guide the material design for optimizing the dispersion in the effective permeability.

Another strategy to assemble nanoparticles is the use of liquid crystals. One way to do so is to simply mix nanoparticles into liquid crystals.^[39] However, using this strategy it is difficult to reach high filling fractions. We followed another approach by directly attaching liquid-crystalline dendrimers bearing cyanobiphenyl moieties to gold nanoparticles using thiols as anchors. The size of the particles has to be adapted to the size of the mesogens and therefore we prepared relatively small particles (about 2 nm). Different strategies were used to attach the dendrimers to gold nanoparticles. The first approach follows the two-phase method proposed by Brust and coworkers^[40] in which a Au(III) salt is mixed with the dendrimer thiol. This leads to a Au(I)-thiol polymer. In the following reduction step the gold is reduced to the metallic state and particles covered by the dendrimer are formed according to a nucleation – growth – passivation mechanism.

Transmission electron microscopy (TEM, Fig. 8) revealed that the particles self-assembled into rows on the graphite film used to perform TEM measurements.^[41] This finding is a proof of concept for the strategy to organize gold particles through the adsorption of dendrimers. The separation between the lines of particles is about 7 nm, whereas one unfolded dendrimer molecule has a length of about 4.6 nm.

The direct synthesis method described above has some disadvantages: The strategy requires large amounts of precious dendrimers and leads to a full coverage of the thiol dendrimer. This is however not necessarily the ideal coverage to induce liquid-crystalline phases. Other methods

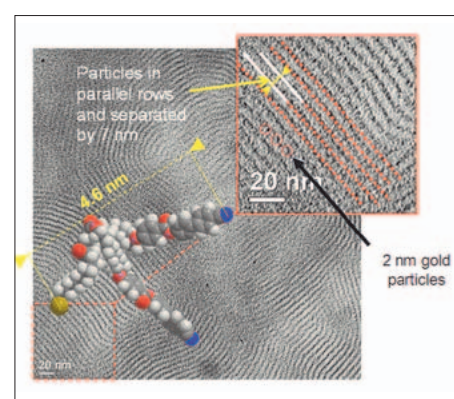


Fig. 8. Transmission electron microscope (TEM) images of nanoparticles covered by dendrimers. The sample was transferred on the TEM grid by simple deposition of a drop of the nanoparticle solution and evaporation of the solvent. Adapted with permission from ref. [41]. Copyright 2008 Wiley VCH.

to introduce dendrimers to gold nanoparticles were therefore used such as thiolate-for-thiolate ligand exchange or chemical reactions like esterification. Some of the materials prepared in this way showed liquid-crystalline phases under the polarized optical microscopy thus revealing a three-dimensional ordering of the gold particles. Today several examples of liquid-crystalline gold are reported and for some the structure has been studied^[42] but their optical properties remain to be investigated.

Gold particles of the size shown in Fig. 8 are intermediate structures between bulk and molecule (atom). Very recently our knowledge on thiol-passivated gold nanoparticles or clusters containing on the order of several tens of gold atoms and thiolate ligands only has drastically deepened due to the determination of the structure of several particles by X-ray crystallography^[3] and the better understanding of the electronic structure of the particles.^[43]

Interestingly, some of the particles are chiral, which directly leads to the following research topic.

Chirality

Chirality plays a crucial role in nature. Furthermore homochirality has drastic consequences in pharmaceutical sciences because enantiomers can behave completely differently in a metabolism. Therefore chemists have to be able to selectively produce one enantiomer of a chiral compound instead of a racemic mixture. Furthermore, the separation of enantiomers and their selective detection are key issues. All these processes require chiral materials. A unique property of a chiral molecule or surface is its ability to discriminate between enantiomers. We seek to understand enantioselection by surfaces and we have therefore designed an experimental approach, absolute configuration modulation spectroscopy, which allowed us to selectively study enantiodiscriminating interactions at chiral solid–liquid interfaces that are responsible for enantioselection on chiral stationary phases.^[10a,b] The goal is to understand how a chiral surface (*e.g.* stationary phase) can discriminate between the enantiomers of a probe molecule and to know which functional groups and intermolecular interactions are responsible for discrimination. This is a formidable task since interactions in such a system are manifold and conventional spectroscopy is usually not able to discriminate between specific (enantiodiscriminating) and non-specific interactions.

Absolute configuration modulation makes use of all the benefits of MES explained above. The power of the method was first demonstrated by studying the interaction of a chiral molecule, ethyl lactate, with a chiral stationary phase (CSP) used in chiral chromatography (Fig. 9). The latter consisted of amylose tris[(*S*)- α -methylbenzylcarbamate] polymer fixed onto silica. A thin film of this material was immobilized on a reflection element for ATR-IR spectroscopy. Solutions of the two enantiomers of ethyl lactate were then flowed alternately over the CSP using a dedicated flow-through cell. Therefore, the external parameter that is modulated in the system is the absolute configuration of ethyl lactate (absolute configuration modulation). ATR-IR spectra were recorded over several modulation cycles and the time-dependent spectra were demodulated according to Eqn. (3). Fig. 9 shows some demodulated spectra for two different experiments. In one experiment (top spectra in Fig. 9) no chiral information was available. The reflection element was covered only by silica. In the demodulated

spectra no signals are observed. To understand this behavior one has to recall that in the demodulated spectra only the periodically changing signals (at the frequency of the stimulation) are observed. Since the two dissolved enantiomers of ethyl lactate show identical infrared spectra no signals are observed after demodulation. The spectra of the two enantiomers remain identical for adsorption on non-chiral sites that cannot discriminate between them. Therefore non-specific interactions do not lead to signals in the demodulated spectra. If the two enantiomers of ethyl lactate however adsorb on sites that can discriminate between them (chiral sites) then the interaction complexes are diastereomers and the corresponding spectra are no longer identical. The differences might be small but these small differences are amplified by the phase-sensitive detection. Some demodulated spectra of such an experiment are shown in Fig. 9 (bottom traces). The signals revealed which functional groups are involved in the enantioselection. Spectral shifts showed that the carbamate groups of the chiral stationary phase served as hydrogen bond donor (N–H) and acceptor (C=O). The ester and O–H group of ethyl lactate in turn served as hydrogen bond acceptor and donor. The spectral shift of the N–H bending mode of the chiral stationary phase and the C=O stretching mode of the lactate were larger for *D*-ethyl lactate than for *L*-ethyl lactate. This indicates that the N–H...O=C hydrogen bonding interaction is stronger in the case of *D*-ethyl lactate. The spectra furthermore indicated that more than one interaction mode is populated and that one side chain of the amylose derivative is stronger involved in the chiral selection than the other two.^[10a] By using the absolute configuration modulation technique enantiodiscrimination at

chiral self-assembled monolayers was also studied.^[10c,44]

In view of the importance of chirality it is not surprising that chiral metal surfaces have gained increasing interest in fundamental research in the last few years.^[45] The use of chirally-modified metal catalysts is a promising strategy for the synthesis of optically pure compounds.^[46] The chirality of metal surfaces can arise at different levels. Many ideal high Miller index single crystal metal surfaces are intrinsically chiral and enantiopure. The chirality in these cases is associated with kink sites and it has been shown that these kinks can differentiate between enantiomers of a compound.^[45a] Through adsorption of molecules a non-chiral metal surface may become chiral as well.

Metal nanoparticles can be viewed as the nanometer size analogues of extended metal surfaces. It should therefore be possible to impart chirality onto the metal particles through adsorption of chiral molecules. In contrast to surfaces the particles can be dissolved and investigated by chiroptical techniques.^[47] Recently the structure of a cluster containing 102 gold atoms and 44 *p*-mercaptobenzoic acid (*p*-MBA) ligands was determined by X-ray crystallography.^[3] Interestingly, the Au₁₀₂p-MBA₄₄ cluster is chiral although *p*-MBA is not. The two enantiomers of the cluster form a racemic crystal. The central gold atoms of the cluster are packed in a Marks decahedron. The structure of the surface region of this cluster is however completely unexpected. In sharp contrast to the textbook knowledge on the structure of self-assembled monolayers of thiolates on gold the surface region of the cluster comprises ‘staples’ (SR–Au–SR, R representing the organic part). The latter resemble Au–thiolate polymers. The gold atoms within these

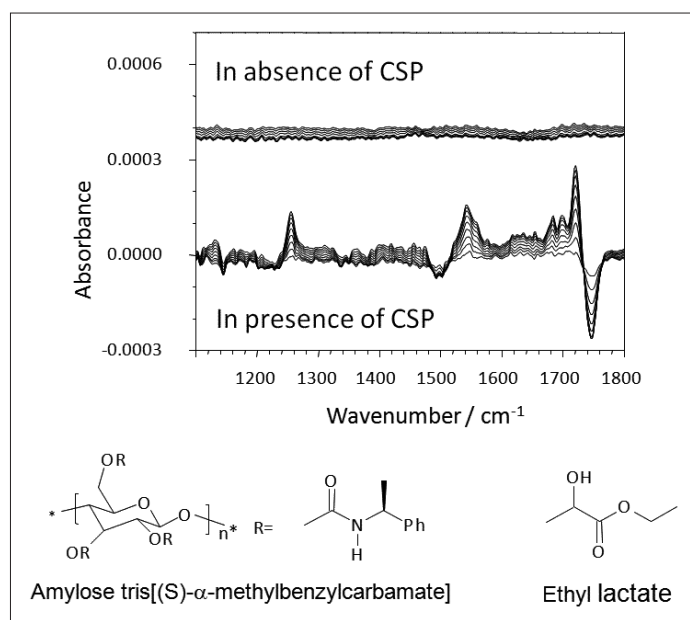


Fig. 9. Demodulated ATR-IR spectra of two absolute configuration modulation experiments. In the first experiment (top traces) no chiral information was present. In the bottom spectra a chiral stationary phase (CSP, amylose tris[(*S*)- α -methylbenzylcarbamate]) was present that could differentiate between the two enantiomers of ethyl lactate. Adapted with permission from ref. [10a]. Copyright 2003 American Chemical Society.

staples are detached from the compact gold core. Some long staples (SR–Au–SR–Au–SR) were also found on the cluster.

The chirality of the cluster arises at two levels: First, within the staples most sulphur atoms are stereogenic centers surrounded by four different ‘groups’, *i.e.* a gold atom of the dense gold core, a gold atom that bridges two sulphur atoms (detached from the gold core), the organic rest R and the free electron pair. Within one cluster 22 sulphur centres have one handedness, 18 have opposite configuration and 2 have no readily assigned chirality. Second, the arrangement of the gold atoms in the surface of the particle is chiral.

More recently the structure of a $\text{Au}_{38}(\text{SC}_2\text{H}_4\text{Ph})_{24}$ cluster was resolved ($\text{HSC}_2\text{H}_4\text{Ph}$, phenylethanethiol) and also in this case the staple motifs were found (Fig. 10).^[48] The $\text{Au}_{38}(\text{SC}_2\text{H}_4\text{Ph})_{24}$ cluster is elongated and the two ends of the cluster are capped by three long staples (SR–Au–SR–Au–SR) which are arranged in a chiral propeller-like structure. The middle part of the cluster is protected by short staples (SR–Au–SR). In the crystal both enantiomers of particles are found. Note that again the protecting thiol is not chiral.

Starting from such $\text{Au}_{38}(\text{SC}_2\text{H}_4\text{Ph})_{24}$ clusters we performed ligand exchange reactions (thiolate-for-thiolate exchange)^[49] by exposing the clusters in solution to an excess of a free thiol. As thiols were chosen BINAS (1,1'-binaphthyl-2,2'-dithiol) and thiophenol and the course of the reaction was followed by MALDI-TOF mass spectrometry. After some time (hours) different species were detected by mass spectrometry corresponding to clusters differing in the number of exchanged ligands. For BINAS, a dithiol, it was observed that two phenylethanethiol ligands were exchanged per BINAS molecule, leading to clusters $\text{Au}_{38}(\text{SC}_2\text{H}_4\text{Ph})_x(\text{BINAS})_y$ ($2y + x = 24$). More interestingly, the exchange stopped at three BINAS molecules (Fig. 11). For thiophenol, a monothiol, the exchange went further to higher numbers of exchanged ligands. This led us to conclude (actually even before the crystal structure of $\text{Au}_{38}(\text{SC}_2\text{H}_4\text{Ph})_{24}$ was known) that BINAS can only exchange on the three short staples. Interestingly, for a $\text{Au}_{40}(\text{SC}_2\text{H}_4\text{Ph})_{24}$ cluster, the structure of which is not yet known, the exchange also went further than three exchanged BINAS ligands, indicating that this cluster has more than three short staples. These results on ligand exchange reactions strongly indicate that site-selective thiolate-for-thiolate ligand exchange reactions can be achieved.

The CD spectra of the partially exchanged $\text{Au}_{38}(\text{SC}_2\text{H}_4\text{Ph})_x(\text{BINAS})_y$ clusters were also measured and the observed optical activity was surprisingly strong after ligand exchange of only few chiral

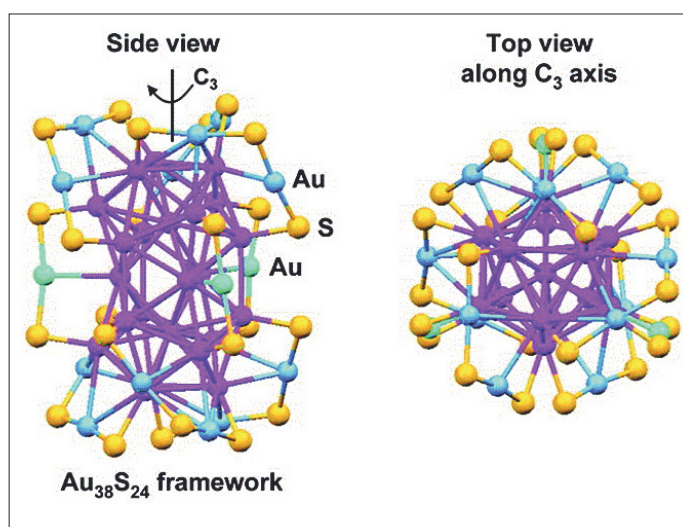


Fig. 10. Structure of $\text{Au}_{38}(\text{SC}_2\text{H}_4\text{Ph})_{24}$ cluster as determined by X-ray crystallography. Color code: Pink corresponds to Au atoms in the dense core, blue and green corresponds to Au atoms in the surface (blue: long staples, green: short staples) and yellow corresponds to sulphur atoms. The organic part is omitted for clarity. Adapted with permission from ref. [48]. Copyright 2010 American Chemical Society.

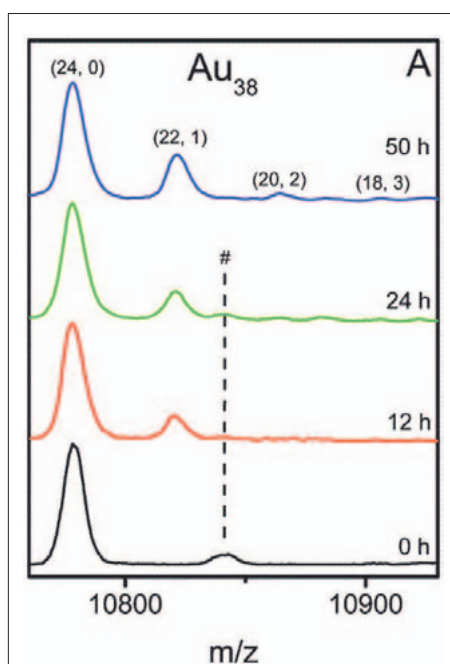


Fig. 11. MALDI mass spectra of Au_{38} signal set as a function of time (0, 12, 24, 50 h) during ligand exchange with BINAS. The assignment of the signals is as follows: (x, y) corresponds to number of 2-ethanethiol and BINAS ligands. # denotes fragments. Adapted with permission from ref. [49]. Copyright 2010 American Chemical Society.

BINAS ligands (Fig. 12^[49]). Optical activity could already be detected at average numbers of BINAS ligands y below one. One possibility to explain this observation is that BINAS imparts its chirality to the overall cluster.

In gold nanoclusters, the staple motifs contain an intrinsic stereochemistry that is overall racemic for achiral thiolates. In short staples (SR–Au–SR) the organic part R of the two thiolates SR can be oriented *cis* or *trans* which are diastereomeric and should differ in their physical properties. Introduction of BINAS into these staples might induce preferred configurations to other staples in its surrounding or it might

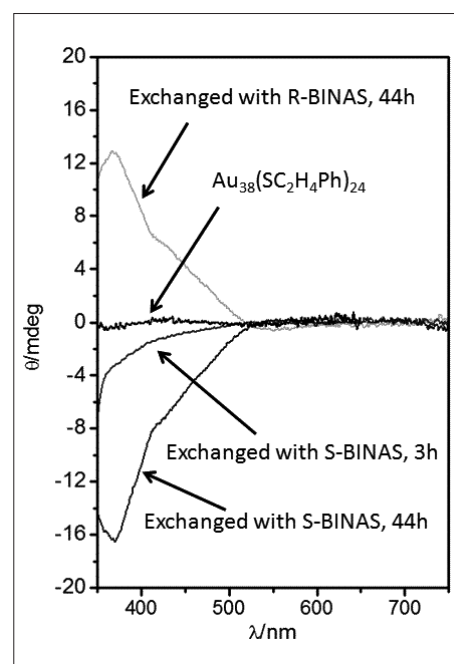


Fig. 12. CD spectra of $\text{Au}_{38}(\text{SC}_2\text{H}_4\text{Ph})_{24}$ and after ligand exchange with BINAS. Adapted with permission from ref. [49]. Copyright 2010 American Chemical Society.

even influence the arrangement of the staples on the cluster surface. Therefore, an enrichment of one of the enantiomers of Au_{38} itself under the induction of an enantiopure ligand (BINAS) seems plausible. This requires certain flexibility for rearrangement of the whole cluster or at least of the staples on the cluster surface. Similar rearrangements have been reported for flat (non chiral) adsorbate-covered surfaces. Some molecules tend to form ordered adsorbate patterns, which may destroy the symmetry of the metal surface underneath.^[50] This results in a supramolecular chirality. In fact, the molecules themselves do not even need to be chiral in this case, which

leads to a globally racemic surface with locally enantiopure patches.^[51] In such a situation the addition of a small amount of a chiral enantiopure compound may force the complete surface to adopt one handedness.^[52] Therefore a few molecules (sergeants) are able to dictate the arrangement of all the other non-chiral molecules (soldiers).

If such effects are operational also in nanoparticles and clusters and to what extent remains to be shown. However, another experimental finding is in agreement with such an effect. Thiolate-for-thiolate ligand exchange was performed on a Au₁₅ cluster that initially contained 13 N-isobutyryl-D-cysteine ligands.^[47d] The cluster was isolated by gel electrophoresis and showed circular dichroism in electronic transitions that are largely associated with the metal. This cluster, the structure of which is not yet known, was then exposed to the other enantiomer of the ligand, *i.e.* N-isobutyryl-L-cysteine in solution. A fast inversion of the CD spectrum was observed (Fig. 13). The shape of the spectrum was retained and the anisotropy factor ($\Delta A/A$) depended on the enantiomeric excess of the N-isobutyryl-cysteine in the system (initially adsorbed thiolate plus added free thiol). The surprising observation was however the fast rate at which the CD spectrum changed. As shown in Fig. 13 the CD signals were inverted already two minutes after addition of the free thiol. Substantial ligand exchange is normally observed after tens of minutes or hours under these conditions.^[53] This could mean that the change in the CD signal (Fig. 13) does not simply reflect the ligand exchange rate, which is supposed to be slower, but rather the change in overall (chiral) structure of the cluster from one enantiomeric form to the other, induced by the presence of few exchanged ligands of opposite absolute configuration. This effect remains however to be investigated in more detail in the future.

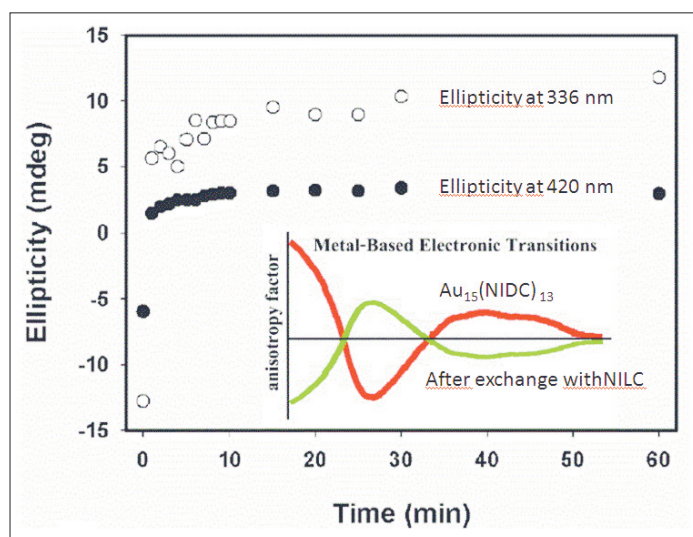


Fig. 13. Ellipticity as a function of time for Au₁₅ cluster covered with N-isobutyryl-D-cysteine (NIDC) after exposing to N-isobutyryl-L-cysteine (NILC). The wavelength-dependent anisotropy factor before and after exchange is also shown. Adapted with permission from ref. [49d]. Copyright 2008 American Chemical Society.

To study the chiral nanoparticles and clusters we used, among other techniques, also vibrational circular dichroism (VCD), *i.e.* the differential absorption of left- and right-circularly polarized infrared light. The technique is analogous to the more popular circular dichroism (CD) spectroscopy in the visible and UV spectral region. However, in contrast to CD, which deals with electronic transitions, VCD deals with molecular vibrations. We used VCD in the past to determine the absolute configuration of organic molecules.^[54] More importantly we also showed that the gold particles exhibit significant vibrational circular dichroism (VCD) signals associated with the adsorbed chiral thiols.^[47c,55] This allowed us, in combination with density functional theory calculations, to determine the structure, *i.e.* conformation, of the adsorbate. This is particularly valuable since methods to determine the structure of molecules adsorbed on nanoparticles are rare. VCD spectra are very sensitive to the conformation of a molecule. The comparison between experimental and calculated spectra for different conformers allows one to extract structural information. As an example Fig. 14 shows VCD spectra for BINAS adsorbed on small gold clusters. The good agreement between experiment and theory shows that VCD is a powerful tool to study the structure of chiral molecules adsorbed on metal particles.^[55b]

For the gold particles covered by (*R*)- and (*S*)-BINAS, respectively, both circular dichroism (CD) and vibrational circular dichroism (VCD) could be measured for different particle sizes separated by size exclusion chromatography.^[55b] The particles covered by enantiomers of BINAS showed mirror image relationship. Whereas the CD spectra strongly depended on the size of the particles the VCD spectra were merely size independent. The CD spectra reflect the electronic structure of the nanoparticles or clusters, which is

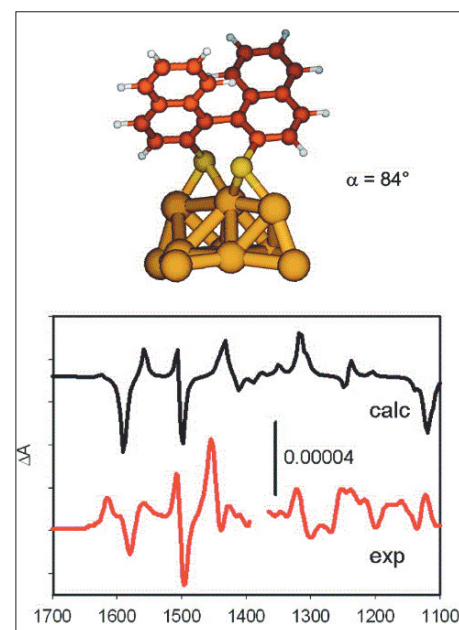


Fig. 14. Comparison between calculated (top) and experimental (bottom) VCD spectra of (*R*)-BINAS adsorbed on gold particles. Calculations were performed at the B3PW91/6-31G(d,p) (LanL2DZ) level of theory. The model of BINAS adsorbed on a small gold cluster used for the calculations is also shown. α is the angle between the naphthyl planes. Adapted with permission from ref. [55b]. Copyright 2008 American Chemical Society.

size dependent. In contrast, the vibrational properties are local, associated with individual adsorbed molecules and therefore the VCD spectra do not strongly depend on the size of the gold particles. This justifies the model used for the calculation of the VCD spectra, which relies on one single adsorbed molecule instead of a cluster comprising several tens of molecules. Unfortunately, the Au-S vibrations of the stereochemically important anchoring part of the thiolates are currently not accessible by VCD measurements. In future Raman optical activity (ROA)^[56] might be used to study chiral nanoparticles in more detail.

Acknowledgements

Part of the work outlined above was supported by the Swiss National Science Foundation (grants PP002-68678, 200021-109176, PP002-116888), by KTI/CTI under project No. P. 8074.1 NMPP-N, by the European Union FP7 project NANOGOLD and by the World Gold Council GROW program. The results summarized above is the product of hard work conducted by past and present coworkers at ETH-Zürich and at the Universities of Neuchâtel, Heidelberg and Geneva and I wish to thank them all.

Received: February 11, 2011

[1] a) M. Studer, H. U. Blaser, C. Exner, *Adv. Synth. Catal.* **2003**, 345, 45; b) A. Baiker, *J. Mol. Catal. A-Chem.* **1997**, 115, 473.

- [2] V. Humblot, S. Haq, C. Muryn, W. A. Hofer, R. Raval, *J. Am. Chem. Soc.* **2002**, *124*, 503.
- [3] P. D. Jadzinsky, G. Calero, C. J. Ackerson, D. A. Bushnell, R. D. Kornberg, *Science* **2007**, *318*, 430.
- [4] B. M. Weckhuysen, *Chem. Commun.* **2002**, 97.
- [5] D. Baurecht, G. Reiter, N. Hassler, M. Schwarzott, U. P. Fringeli, *Chimia* **2005**, *59*, 226.
- [6] a) N. J. Harrick, *J. Phys. Chem.* **1960**, *64*, 1110; b) J. Fahrenfort, *Spectrochim. Acta* **1961**, *17*, 698.
- [7] D. Baurecht, U. P. Fringeli, *Rev. Sci. Instr.* **2004**, *72*, 3782.
- [8] a) T. Burgi, A. Baiker, *J. Phys. Chem. B* **2002**, *106*, 10649; b) T. Burgi, A. Baiker, *Adv. Catal.* **2006**, *50*, 227; c) N. Bonalumi, T. Burgi, A. Baiker, *J. Am. Chem. Soc.* **2003**, *125*, 13342; d) A. Urakawa, T. Bürgi, H.-P. Schläpfer, A. Baiker, *J. Chem. Phys.* **2006**, *124*, Art. No 054717; e) T. Burgi, M. Bieri, *J. Phys. Chem. B* **2004**, *108*, 13364.
- [9] M. Bieri, T. Burgi, *Langmuir* **2005**, *21*, 1354.
- [10] a) R. Wirz, T. Burgi, A. Baiker, *Langmuir* **2003**, *19*, 785; b) R. Wirz, T. Bürgi, W. Lindner, A. Baiker, *Anal. Chem.* **2004**, *76*, 5319; c) M. Bieri, T. Burgi, *J. Phys. Chem. B* **2005**, *109*, 10243.
- [11] I. Dolamic, T. Bürgi, *J. Phys. Chem. B* **2006**, *110*, 14898.
- [12] I. Dolamic, T. Bürgi, *J. Catal.* **2007**, *248*, 268.
- [13] I. Dolamic, T. Bürgi, *J. Phys. Chem. C* **2011**, *115*, 2228.
- [14] H. Hidaka, S. Horikoshi, K. Ajsaka, J. Zhao, N. Serpone, *J. Photochem. Photobiol. A-Chem.* **1997**, *108*, 197.
- [15] B. Oregan, M. Gratzel, *Nature* **1991**, *353*, 737.
- [16] a) T. J. Meyer, *Nature* **2008**, *451*, 778; b) N. D. McDaniel, F. J. Coughlin, L. L. Tinker, S. Bernhard, *J. Am. Chem. Soc.* **2008**, *130*, 210.
- [17] L. Tong, Y. Zhao, T. B. Huff, M. N. Hansen, A. Wei, J. X. Cheng, *Adv. Mater.* **2007**, *19*, 3136.
- [18] a) C. Wang, J. Irudayaraj, *Small* **2008**, *4*, 2204; b) P. K. Sudeep, S. T. S. Joseph, K. G. Thomas, *J. Am. Chem. Soc.* **2005**, *127*, 6516.
- [19] H. Ding, K. T. Yong, I. Roy, H. E. Pudavar, W. C. Law, E. J. Bergey, P. N. Prasad, *J. Phys. Chem. C* **2007**, *111*, 12552.
- [20] J. W. M. Chon, C. Bullen, P. Zijlstra, M. Gu, *Adv. Funct. Mater.* **2007**, *17*, 875.
- [21] a) N. Shalkevich, W. Escher, T. Burgi, B. Michel, L. Si-Ahmed, D. Poulidakos, *Langmuir* **2010**, *26*, 663; b) N. Shalkevich, A. Shalkevich, T. Burgi, *J. Phys. Chem. C* **2010**, *114*, 9568.
- [22] C. Rockstuhl, F. Lederer, C. Etrich, T. Pertsch, T. Scharf, *Phys. Rev. Lett.* **2007**, 99.
- [23] P. Mulvaney, *Langmuir* **1996**, *12*, 788.
- [24] C. Gautier, A. Cunningham, L. Si-Ahmed, G. Robert, T. Burgi, *Gold Bull.* **2010**, *43*, 94.
- [25] N. R. Jana, L. Gearheart, C. J. Murphy, *Adv. Mater.* **2001**, *13*, 1389.
- [26] W. Stober, A. Fink, E. Bohn, *J. Colloid Interface Sci.* **1968**, *26*, 62.
- [27] Q. L. Li, T. Burgi, H. Chen, *J. Wuhan Univ. Technol.-Mat. Sci. Edit.* **2010**, *25*, 104.
- [28] E. P. Barrett, L. G. Joyner, P. P. Halenda, *J. Am. Chem. Soc.* **1951**, *73*, 373.
- [29] C. T. Kresge, M. E. Leonowicz, W. J. Roth, J. C. Vartuli, J. S. Beck, *Nature* **1992**, *359*, 710.
- [30] P. Zijlstra, J. W. M. Chon, M. Gu, *Nature* **2009**, *459*, 410.
- [31] V. G. Veselago, *Soviet Physics Uspekhi-Ussr* **1968**, *10*, 509.
- [32] D. R. Smith, J. B. Pendry, M. C. K. Wiltshire, *Science* **2004**, *305*, 788.
- [33] C. R. Simovski, S. A. Tretyakov, *Phys. Rev. B* **2009**, 79.
- [34] a) V. Yannopoulos, *Appl. Phys. A-Mater. Sci. Process.* **2007**, *87*, 259; b) V. A. Tamma, J. H. Lee, Q. Wu, W. Park, *Appl. Optics* **2010**, *49*, A11.
- [35] N. Shalkevich, A. Shalkevich, L. Si-Ahmed, T. Burgi, *Phys. Chem. Chem. Phys.* **2009**, *11*, 10175.
- [36] G. Frens, *Nature-Physical Science* **1973**, *241*, 20.
- [37] Y. L. Xu, *Appl. Optics* **1995**, *34*, 4573.
- [38] S. Mühlig, C. Rockstuhl, V. Yannopoulos, T. Bürgi, N. Shalkevich, F. Lederer, manuscript in preparation **2011**.
- [39] T. Hegmann, H. Qi, V. M. Marx, *J. Inorg. Organomet. Polym. Mater.* **2007**, *17*, 483.
- [40] M. Brust, M. Walker, D. Bethell, D. J. Schiffrin, R. Whyman, *J. Chem. Soc. Chem. Commun.* **1994**, 801.
- [41] S. Frein, J. Boudon, M. Vonlanthen, T. Scharf, J. Barbera, G. Süss-Fink, T. Burgi, R. Deschenaux, *Helv. Chim. Acta* **2008**, *91*, 2321.
- [42] a) L. Cseh, G. H. Mehl, *J. Am. Chem. Soc.* **2006**, *128*, 13376; b) X. B. Zeng, F. Liu, A. G. Fowler, G. Ungar, L. Cseh, G. H. Mehl, J. E. Macdonald, *Adv. Mater.* **2009**, *21*, 1746; c) M. Wojcik, W. Lewandowski, J. Matraszek, J. Mieczkowski, J. Borysiuk, D. Pocięcha, E. Gorecka, *Angew. Chem. Int. Ed.* **2009**, *48*, 5167.
- [43] M. Walter, J. Akola, O. Lopez-Acevedo, P. D. Jadzinsky, G. Calero, C. J. Ackerson, R. L. Whetten, H. Gronbeck, H. Hakkinen, *Proc. Natl. Acad. Sci. U. S. A.* **2008**, *105*, 9157.
- [44] M. Bieri, T. Bürgi, *Chem. Phys. Chem.* **2006**, *7*, 514.
- [45] a) C. F. McFadden, P. S. Cremer, A. J. Gellman, *Langmuir* **1996**, *12*, 2483; b) R. Fasel, M. Parschau, K. H. Ernst, *Nature* **2006**, *439*, 449.
- [46] T. Bürgi, A. Baiker, *Acc. Chem. Res.* **2004**, *37*, 909.
- [47] a) T. G. Schaaff, R. L. Whetten, *J. Phys. Chem. B* **2000**, *104*, 2630; b) H. Yao, K. Miki, N. Nishida, A. Sasaki, K. Kimura, *J. Am. Chem. Soc.* **2005**, *127*, 15536; c) C. Gautier, T. Burgi, *J. Am. Chem. Soc.* **2006**, *128*, 11079; d) C. Gautier, T. Burgi, *J. Am. Chem. Soc.* **2008**, *130*, 7077; e) C. Gautier, T. Burgi, *ChemPhysChem* **2009**, *10*, 483.
- [48] H. F. Qian, W. T. Eckenhoff, Y. Zhu, T. Pintauer, R. C. Jin, *J. Am. Chem. Soc.* **2010**, *132*, 8280.
- [49] S. Knoppe, A. C. Dharmaratne, E. Schreiner, A. Dass, T. Burgi, *J. Am. Chem. Soc.* **2010**, *132*, 16783.
- [50] M. O. Lorenzo, S. Haq, T. Bertrams, P. Murray, R. Raval, C. J. Baddeley, *J. Phys. Chem. B* **1999**, *103*, 10661.
- [51] V. Humblot, M. O. Lorenzo, C. J. Baddeley, S. Haq, R. Raval, *J. Am. Chem. Soc.* **2004**, *126*, 6460.
- [52] M. Parschau, S. Romer, K. H. Ernst, *J. Am. Chem. Soc.* **2004**, *126*, 15398.
- [53] R. Guo, Y. Song, G. L. Wang, R. W. Murray, *J. Am. Chem. Soc.* **2005**, *127*, 2752.
- [54] a) D. Bas, T. Burgi, J. Lacour, J. Vachon, J. Weber, *Chirality* **2005**, *17*, S143; b) C. Herse, D. Bas, F. C. Krebs, T. Burgi, J. Weber, T. Wesolowski, B. W. Laursen, J. Lacour, *Angew. Chem. Int. Ed.* **2003**, *42*, 3162; c) P. Mobian, C. Nicolas, E. Francotte, T. Burgi, J. Lacour, *J. Am. Chem. Soc.* **2008**, *130*, 6507; d) T. Burgi, A. Urakawa, B. Behzadi, K. H. Ernst, A. Baiker, *New J. Chem.* **2004**, *28*, 332.
- [55] a) C. Gautier, T. Burgi, *Chem. Commun.* **2005**, 5393; b) C. Gautier, T. Burgi, *J. Phys. Chem. C* **2010**, *114*, 15897.
- [56] J. Haesler, W. Hug, *Chimia* **2008**, *62*, 482.